





Cite this: *Soft Matter*, 2020, 16, 6063

Enzymatically degradable, starch-based layer-by-layer films: application to cytocompatible single-cell nanoencapsulation†

Hee Chul Moon,^a Sol Han,^a João Borges,^b Tamagno Pesqueira,^b Hyunwoo Choi,^a Sang Yeong Han,^a Hyeoncheol Cho,^a Ji Hun Park,^c João F. Mano *^b and Insung S. Choi *^a

The build-up and degradation of cytocompatible nanofilms in a controlled fashion have great potential in biomedical and nanomedicinal fields, including single-cell nanoencapsulation (SCNE). Herein, we report the fabrication of biodegradable films of cationic starch (c-ST) and anionic alginate (ALG) by electrostatically driven layer-by-layer (LbL) assembly technology and its application to the SCNE. The [c-ST/ALG] multilayer nanofilms, assembled either on individual *Saccharomyces cerevisiae* or on the 2D flat gold surface, degrade on demand, in a cytocompatible fashion, *via* treatment with α -amylase. Their degradation profiles are investigated, while systematically changing the α -amylase concentration, by several surface characterization techniques, including quartz crystal microbalance with dissipation monitoring (QCM-D) and ellipsometry. DNA incorporation in the LbL nanofilms and its controlled release, upon exposure of the nanofilms to an aqueous α -amylase solution, are demonstrated. The highly cytocompatible nature of the film-forming and -degrading conditions is assessed in the c-ST/ALG-shell formation and degradation of *S. cerevisiae*. We envisage that the cytocompatible, enzymatic degradation of c-ST-based nanofilms paves the way for developing advanced biomedical devices with programmed dissolution *in vivo*.

Received 13th May 2020,
Accepted 2nd June 2020

DOI: 10.1039/d0sm00876a

rsc.li/soft-matter-journal

Introduction

Layer-by-layer (LbL) films with degradable characteristics have been fabricated for various applications including drug delivery, tissue engineering, and prosthetic devices.^{1–4} In biomedical applications, the materials to be employed in the LbL process should be compatible with biological entities (*e.g.*, proteins and cells).^{5–7} The biocompatible materials and their assemblies also have recently caught significant attention in the emerging field of single-cell nanoencapsulation (SCNE).^{8–11} The biocompatible LbL films could also act as a reaction platform for postfunctionalization, exemplified by SiO₂ or TiO₂ formation under physiologically relevant conditions.^{12–15}

Nature-derived biopolymers are strong candidates for the cytocompatible LbL assembly.^{16,17} Among them, marine polysaccharides, such as alginic acid, chitosan, chondroitin sulfate,

heparin, and hyaluronic acid, have widely been employed in the formation of LbL films because of their diversity in chemical composition, properties, and functions.¹⁸ In particular, the varied charge identities in marine polysaccharides make them highly suitable for electrostatically driven LbL process.^{19,20} For instance, alginic acid is negatively charged at the neutral pH,^{21,22} and chitosan is positively charged under mild acidic conditions.^{23,24} In comparison, starch (ST), the most abundant polysaccharide in the plant, has scarcely been used for the formation of LbL films due to its low charge density.^{25–27}

ST is mainly composed of amylose and amylopectin.²⁸ Amylose is an $\alpha(1 \rightarrow 4)$ -linked, linear polymer of α -D-glucose,^{29,30} and amylopectin is a branched, α -D-glucose-based polymer with additional $\alpha(1 \rightarrow 6)$ -glycosidic bonds for branching.³¹ ST degrades into monomers, dimers, and oligomers, in the organism, by the action of various enzymes.³² For example, α -amylase, present in the pancreas and salivary gland, randomly hydrolyzes the $\alpha(1 \rightarrow 4)$ -glycosidic bonds and breaks the ST chain down to dextrans, maltose, and glucose. Amyloglucosidase, found in the small intestine, hydrolyzes the $\alpha(1 \rightarrow 4)$ -glycosidic bonds at the non-reducing ends of the ST. Isoamylase is an isoenzyme of α -amylase and cleaves the $\alpha(1 \rightarrow 6)$ -glycosidic bonds of the ST. The plant has β -amylase, which hydrolyzes $\alpha(1 \rightarrow 4)$ -glycosidic

^a Center for Cell-Encapsulation Research, Department of Chemistry, KAIST, Daejeon 34141, Korea. E-mail: ischoi@kaist.ac.kr

^b Department of Chemistry, CICECO-Aveiro Institute of Materials, University of Aveiro, Campus Universitário de Santiago, 3810-193 Aveiro, Portugal. E-mail: jmano@ua.pt

^c Department of Science Education, Ewha Womans University, Seoul 03760, Korea

† Electronic supplementary information (ESI) available. See DOI: 10.1039/d0sm00876a

bonds at every 2 glucose units to produce maltose only, in the vacuole and mesophyll cell chloroplasts. Numerous microbes produce the amylases aforementioned, and these microbial amylases are active under harsh conditions, such as high temperature, and acidic and basic solutions.

The enzymatic biodegradation of the ST has led to numerous studies on its applications to the food packaging and paper manufacturing.³³ In the biomedical and nanomedicinal fields, ST-based polymers also would be better functional and more versatile, compared with the polysaccharides mainly derived from marine species, by considering the presence of the various ST-digestive enzymes in distinct anatomic sites of the human body, as well as in other organisms. Herein, we fabricated α -amylase-driven, enzymatically degradable ST-based LbL films for the SCNE. The precisely controlled degradation of the assemblies was also applied to the enzyme-triggered drug release with DNA as a model. To the best of our knowledge, this is the first report on the development of LbL-assembled nanoshells that degrade under cytocompatible conditions in the SCNE. The enzymatically degradable ST-based LbL multilayers could pave the way towards next-generation devices in a multitude of nanomedicinal, biomedical, and SCNE applications.

Materials and methods

Materials

Starch (ST) from wheat, sodium alginate (ALG), α -amylase from *Aspergillus oryzae*, acetic acid, bisBenzimide H 33258, deoxyribonucleic acid sodium salt from salmon testes (DNA), disodium phosphate, ferric chloride hexahydrate ($\text{FeCl}_3 \cdot 6\text{H}_2\text{O}$), fluorescein diacetate (FDA), glycidyltrimethylammonium chloride, hydrochloric acid (HCl), monosodium phosphate, 3-(*N*-morpholino)propanesulfonic acid (MOPS), propidium iodide (PI), sodium acetate, sodium chloride (NaCl), sodium hydroxide (NaOH), tannic acid (TA), tris(hydroxymethyl)aminomethane hydrochloride (Tris-HCl), and 11-mercaptoundecanoic acid (MUA) were purchased from Sigma-Aldrich. Hydrogen peroxide was purchased from Samchun. Ethylenediaminetetraacetic acid disodium salt (EDTA) and sulfuric acid were purchased from Junsei. Gold substrates were prepared by thermal deposition of titanium (5 nm) and gold (100 nm) onto silicon wafers (Sehyoung Wafertech). Yeast extract peptone dextrose (YPD) agar and YPD broth were purchased from Duchefa Biochemistry. Deionized (DI) water (18.3 M Ω cm) from Milli-Q Direct 8 (Millipore) was used in the preparation of all solutions.

Synthesis of cationic starch (c-ST)

ST was functionalized with glycidyltrimethylammonium chloride via the base-catalyzed, ring-opening reaction to provide cationic charges. Briefly, ST (1.5 g) was dissolved in 150 mL of DI water and stirred at 90 °C for 1 h. NaOH (0.5 g) was then added to the ST solution, followed by dropwise addition of a glycidyltrimethylammonium chloride solution (591 μL , 90%). The resulting solution was kept at 70 °C for 18 h, and 1 M HCl was added to lower the pH value below 7 to terminate the

reaction. The solution was cooled to room temperature, and the polymer was precipitated by adding excess ethanol, dissolved in DI water, dialyzed (molecular-weight cutoff: 3500 Da) for 3 days, and lyophilized for another 3 days. The c-ST was characterized by ^1H nuclear magnetic resonance (NMR) spectroscopy (D_2O , 400 MHz) and elemental analysis.

LbL fabrication of c-ST and ALG on gold

Gold substrates were cut into the square shapes and cleaned with piranha solution (3:1 (v/v) mixture of concentrated sulfuric acid and hydrogen peroxide (30%, v/v)), followed by rinsing thoroughly with DI water and drying under the flow of argon gas. The MUA self-assembled monolayers (SAMs) were formed on the gold substrates by immersing them in a MUA solution in ethanol (1 mM) for 18 h, followed by washing the substrates with ethanol and drying under the flow of argon gas. The MUA-primed gold substrates were immersed in an aqueous c-ST solution (0.1 mg mL⁻¹ in a 0.1 M acetate buffer solution at pH 4.5) for 4 min, washed with the 0.1 M acetate buffer at pH 4.5 for 3 min, immersed in an aqueous ALG solution (0.05 mg mL⁻¹ in the 0.1 M acetate buffer solution at pH 4.5) for 4 min, and washed with the 0.1 M acetate buffer at pH 4.5 for 3 min. The pH value of 4.5 was chosen for the LbL assembly, because the absolute magnitudes of the measured zeta potentials were high and similar to each other at pH 4.5 (+13.10 for c-ST and -15.10 for ALG solutions). This deposition process gave rise to one c-ST/ALG bilayer, and the process was repeated nine times to obtain 9 bilayers.

Quartz crystal microbalance with dissipation monitoring (QCM-D)

The LbL deposition of oppositely charged c-ST and ALG biopolymers was monitored *in situ* by the QCM-D (Q-Sense Pro, Biolin Scientific) in a liquid environment. Freshly cleaned gold-coated AT-cut quartz sensors (QSX301 Gold, Q-Sense) were used as an LbL substrate. The gold-coated quartz sensors were excited at multiple overtones (1st, 3rd, 5th, 7th, 9th, 11th, and 13th, corresponding to 5, 15, 25, 35, 45, 55, and 65 MHz, respectively), and shifts in frequency (Δf) and in energy dissipation (ΔD) were monitored in real-time. The results presented herein corresponded to the Δf and in ΔD associated with the 7th overtone (35 MHz). Nevertheless, the results were representatives of the other overtones. The adsorption process was performed at 25 °C and at a constant flow rate of 50 $\mu\text{L min}^{-1}$ by using aqueous c-ST and ALG solutions at 0.1 mg mL⁻¹ and 0.05 mg mL⁻¹, respectively, in the 0.1 M acetate buffer (pH 4.5). In-between the depositions of the biopolymers, a washing step with the 0.1 M acetate buffer (pH 4.5) was employed to remove weakly adsorbed molecules. The biopolymer and rinsing solutions were flushed for 4 and 3 min, respectively. The film build-up was performed to fabricate five bilayers of [c-ST/ALG]. After fabrication of [c-ST/ALG]₅, an α -amylase solution (1, 20, 300, or 500 $\mu\text{g mL}^{-1}$ in the 0.1 M acetate buffer, pH 5.5) was flushed at a constant flow rate of 50 $\mu\text{L min}^{-1}$ to assess the degradation profile.

DNA release

The DNA from salmon testes (salmon sperm DNA, SS-DNA), as a model biomolecule, was incorporated to the [c-ST/ALG]₄[c-ST/DNA]₅,

multilayer films by performing an additional LbL process to the [c-ST/ALG]_n films. A DNA solution at 0.1 mg mL⁻¹ in the 0.1 M acetate buffer solution (pH 4.5) was used for the LbL assembly process. After assembly process, the multilayer films were allowed to stabilize for 30 min in the 0.1 M acetate buffer solution (pH 4.5), followed by dipping in the α-amylase aqueous solution (20 or 500 μg mL⁻¹ in the 0.1 M acetate buffer (pH 5.5)) for 240 min. The blank acetate buffer was used as a control. An aliquot of 40 μL was collected at the predetermined time point, gently mixed with 400 ng mL⁻¹ of a bisBenzimide H 33258 solution in the 2× TNE buffer (20 mM Tris-HCl, 0.4 M NaCl, and 2 mM EDTA), and the fluorescence intensity was measured by fluorescence spectroscopy (λ_{ex} = 346 nm; λ_{em} = 460 nm). The experiments were performed in triplicate.

Single-cell nanoencapsulation (SCNE)

A single colony of yeast (*Saccharomyces cerevisiae*, ATCC18824) from the YPD agar plate was picked and cultured in YPD broth media with gentle shaking at 33 °C for 30 h. The yeast cells were washed with DI water three times and dispersed in DI water. For priming the cells with the Fe³⁺-TA complex, to an aqueous suspension of yeast cells (490 μL) were added 5 μL of the aqueous TA solution (40 mg mL⁻¹) and 5 μL of the aqueous FeCl₃·6H₂O solution (10 mg mL⁻¹) sequentially with 10 s of vigorous mixing between the additions. After additional vigorous mixing for 10 s, 0.5 mL of MOPS buffer (20 mM, pH 7.4) was added to the cell suspension for the pH stabilization, resulting in the formation of stable Fe³⁺-TA complex. For the LbL-shell assembly of c-ST and ALG, the Fe³⁺-TA-primed yeast cells were washed twice with the phosphate buffer (PB) solution (0.1 M, pH 5.8), and alternately immersed in the PB solutions of c-ST (1.6 mg mL⁻¹) and ALG (or fluorescein-linked ALG (F-ALG)) (0.8 mg mL⁻¹) for 5 min each. After spin-down at 6000 rpm, the cells were washed with the PB solution after each LbL step. The alternate deposition was repeated to form the [c-ST/ALG]_n[c-ST/F-ALG]₃ multilayer nanoshells on *S. cerevisiae*. For the viability assay, 5 μL of the FDA solution (10 mg mL⁻¹ in acetone) and 2 μL of the aqueous PI solution (1 mg mL⁻¹) were added to the yeast suspension (1 mL). The resulting yeast suspension was incubated for 20 min, washed with the PB solution, and characterized by confocal laser-scanning microscopy.

Characterizations

The synthesized c-ST compound was characterized by ¹H NMR spectroscopy (Bruker) operated at the ultrashield of 400 MHz with deuterium oxide. The film thickness was measured with an Elli-SE ellipsometer (Ellipso Technology). The wavelength range of light was 400 to 700 nm, and the film-optimized model system was used for the variable refractive index. Four different points of each sample were measured, and average values were recorded. Fourier-transform infrared (FT-IR) spectra were obtained with a nitrogen-purged Thermo Nicolet Nexus FT-IR spectrophotometer (Thermo Fisher). The spectra were equalized by adding approximately 4000 scans for background and each sample. Atomic force microscopy (AFM) images were taken in tapping mode with an INNOVA-LABRAM HR800 (Horiba Jobin & Bruker). Contact angle

measurements were performed using a Phoenix 300 goniometer (Surface Electro Optics Co.) equipped with a video camera. The static contact angle of a 3 μL water droplet was measured at four different locations on each sample, and average values were recorded. The fluorescent images were obtained with an LSM 700 confocal laser-scanning microscope (Carl Zeiss).

Results and discussion

Synthesis of cationic starch (c-ST)

LbL assembly is one of the most widely and intensively employed bottom-up methodologies for the construction of degradable thin films.^{34–36} It is based on the alternate deposition of materials exhibiting complementary intermolecular interactions, including electrostatic, hydrophobic, or hydrogen bonding interactions. The degradable LbL multilayer films, in principle, could be designed and fabricated on demand with any polymer combinations for substrates of any shapes, if the self-assembling materials for the films have sufficient and specific interactions with each other.

ST would be a promising base material for the formation of degradable LbL films because of its natural abundance, and intrinsic biocompatibility and biodegradability; however, its neutral glucose backbone, having only hydroxyl (–OH) groups, has precluded its wide applicability in the LbL ensembles. In this work, an ST derivative (c-ST), having positive charges on its backbone, was used in the LbL assembly process.³⁷ Wheat ST was heated to 90 °C for gelatinization, loosening its globular structure by releasing strong intramolecular hydrogen bonds, and cationized by the base-catalyzed ring-opening reaction with glycidyltrimethylammonium chloride (Fig. S1a, ESI[†]). The ¹H NMR spectrum showed the characteristic proton peaks for the ST backbone at 5.4 (s, 1H), 3.72–3.84 (m, 4H), 3.54–3.62 (m, 2H), and 3.4–3.48 (m, 2H) ppm, and the peaks from the attached trimethylammonium (–NMe₃⁺) chain were observed at 3.19 (s, 9H) and 4.38 (s, 1H) ppm (Fig. S1b, ESI[†]). The elemental analysis of freeze-dried samples indicated that c-ST contained 1.61% of nitrogen, corresponding to 0.287 of the degree of substitution (Fig. S1c, ESI[†]).

LbL film formation

The LbL-assembled films were fabricated by alternately depositing c-ST and alginate (ALG) onto a gold surface primed with the SAMs of MUA (Fig. 1). The presence of c-ST and ALG in the multilayer films was confirmed by FT-IR spectroscopy (Fig. 2a). The absorption bands for C–O–H, C–O–C, and O–H groups in the c-ST backbone were observed at 1050, 1155, and 1320 cm⁻¹, respectively, and the band of C=O stretching, from the carboxyl groups in the mannuronate and guluronate residues of ALG, appeared at 1600 cm⁻¹. The band intensity increased while increasing the number of bilayers, confirming the successful build-up of the c-ST/ALG multilayer films.

The growth of the multilayer films ([c-ST/ALG]_n) was followed by the ellipsometric-thickness measurement (Fig. 2b). The film thickness was 1.1 nm for [c-ST/ALG]₁ and increased to 24.14 nm for [c-ST/ALG]₉. Fig. 2b also showed the exponential-to-linear

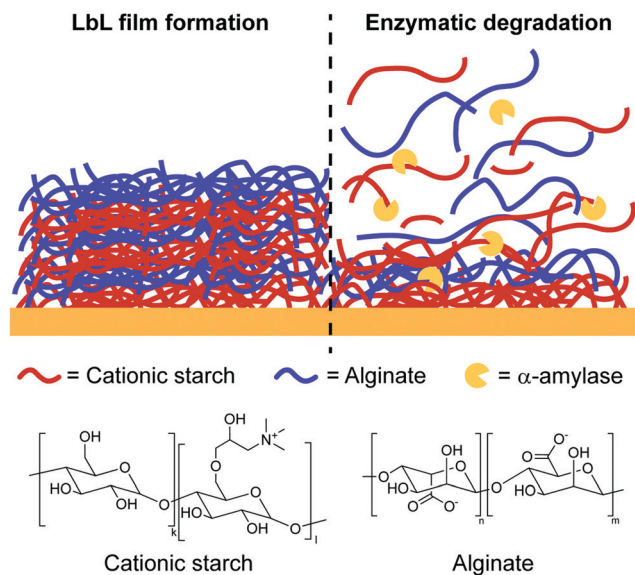


Fig. 1 Schematic representation of the c-ST/ALG LbL film formation and α -amylase-triggered film degradation.

film growth with the number of bilayers, similarly to the previous studies of the poly-glutamic acid- and poly-L-lysine-based LbL films.^{38,39} The observed initial exponential-growth implied that excess of c-ST and/or ALG could freely diffuse into the interior of the multilayer films during the deposition process. The biopolymers in the films could also come out to the film surface and enable the additional adsorption of the incoming biopolymer.¹⁹ The transition to linear growth after 4-bilayer deposition indicated that the deepest region of the multilayer films was reconstructed to limit the free diffusion of the biopolymers, and this densified region also grew with the bilayer deposition, which could maintain the thickness of the diffusible region and induce the linear growth of the films. The existence of free diffusion region in the c-ST/ALG films also implied that the adhesive forces between polymers in the solution and on the film surface were relatively stronger than the cohesive forces between polymers in the films. The strong interactions between c-ST and ALG would lead to the formation of polymeric complex structures upon drying, which was effectively visualized by AFM (Fig. 2c). The AFM images showed that the [c-ST/ALG]₅ films had islet structures, and the root-mean-square roughness (RMS) gradually increased from 1.48 to 3.97 nm with the number of deposited bilayers.

The c-ST/ALG LbL process was further characterized in detail by QCM-D measurements, which allowed for real-time monitoring of the film deposition. Fig. 3 shows the changes in frequency ($\Delta f_7/7$) and dissipation (ΔD_7) shifts at the seventh overtone during the five-bilayer deposition, respectively. The $\Delta f_7/7$ decreased discernably upon the injection of each biopolymer solution (c-ST and ALG), indicating that c-ST and ALG were successfully adsorbed onto the gold-plated quartz crystal substrate. The assembled films were stable, and the introduction of the washing buffer did not cause any frequency changes, thus revealing the irreversible nature of the adsorption process. The $\Delta f_7/7$ data clearly confirmed that the films were formed

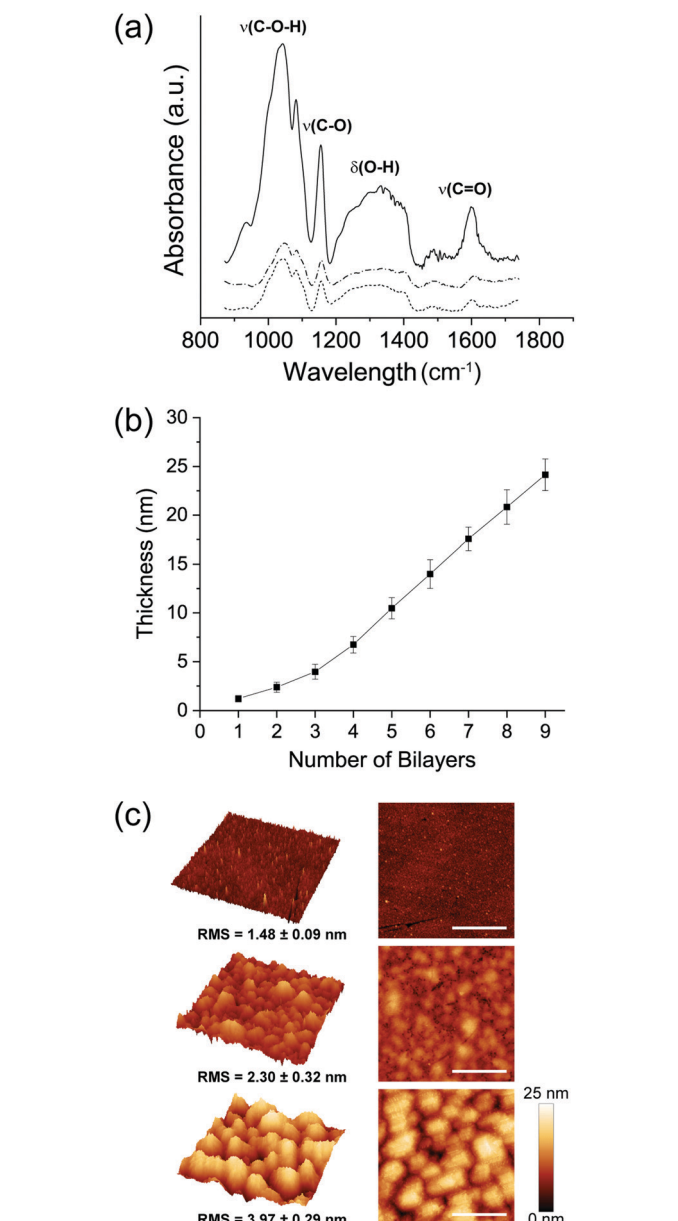


Fig. 2 (a) FT-IR spectra of the [c-ST/ALG]_n multilayer films ($n = 1, 3$ and 5 bilayers). (b) Film thickness vs. number of bilayers. (c) AFM micrographs of bare gold (top), [c-ST/ALG]₃ (middle), and [c-ST/ALG]₅ films (bottom). All scale bars represent 2 μm .

durably from-polymer-by-polymer in the course of five-bilayer deposition steps, making [c-ST/ALG]₅. On the other hand, the observed increase in the ΔD_7 values, which are defined as the sum of the oscillation-energy losses in the system caused by the interaction between the films and the medium, implied that the c-ST/ALG multilayer films interacted strongly with the aqueous solution and had soft and viscous properties. This characteristic was previously observed by us while assembling chitosan and hyaluronic acid multilayers.⁴⁰ The film softness was the result of the strong interaction of the biopolymers with water, as well as of the hydration or swelling of the multilayer films. Accordingly, the water contact angles for [c-ST]₅[ALG]₄ and [c-ST]₅[ALG]₅

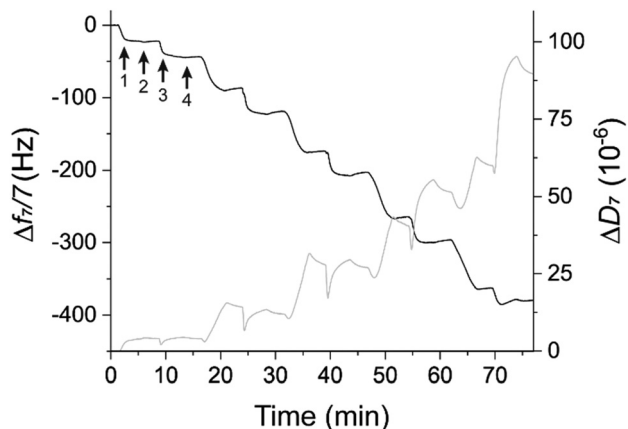


Fig. 3 QCM-D monitoring of the normalized frequency ($\Delta f_n/n$) and dissipation (ΔD_n) shifts, obtained at the 7th overtone ($n = 7$; 35 MHz), as a function of time for the LbL deposition of [c-ST/ALG]₅ bilayers on gold-plated quartz crystal sensors and intermediate rinsing steps. The arrow 1 indicates the injection time for c-ST, and the arrow 3 for ALG. The arrows 2 and 4 indicate the rinsing step with the 0.1 M acetate buffer solution (pH 4.5).

multilayer films were measured to be 18.8° and 15.5°, respectively, compared with 87.5° of the bare gold substrate (Fig. S2, ESI[†]).

Enzymatic degradation

The enzymatic degradation of LbL films has several advantages over other degradation methods. For example, the enzymatic reaction degrades its target molecules selectively and provides spatiotemporal control over the degradation reaction. It also does not affect or harm other surrounding entities and ensures non-toxic or non-inflammatory responses, which is highly beneficial in biomedical applications. Moreover, unlike other hydrolytic reactions, it is much rapid, enabling precise control of degradation characteristics. Because of the substantial advantages, the enzymatic degradation of LbL multilayers has widely been attempted in controlled drug delivery systems and other biomedical applications.^{40–42} More importantly, it would contribute profoundly to the emerging field of the SCNE, where individual living cells are to be encapsulated with cyto-compatible materials, preferably in a reversible fashion.^{8–11}

We investigated the enzymatic-degradation behavior of [c-ST/ALG]₅ films with α -amylase, which randomly cleaves the $\alpha(1 \rightarrow 4)$ -glycosidic bonds. We envisioned that the presence of α -amylase in saliva would lead to the potential development of mouth strips in drug delivery systems.⁴³ The four different α -amylase solutions (concentration: 500, 300, 20, and 1 $\mu\text{g mL}^{-1}$) were prepared in acetate buffer solution (0.1 M, pH 5.5) for the degradation studies. The QCM-D analysis (Fig. 4a) clearly showed that the degradation reaction occurred faster as the enzyme concentration increased. For example, in the case of 500 $\mu\text{g mL}^{-1}$, a very rapid film degradation occurred, and most of the films (88%) were degraded in 15 min. It is important to note that the topmost layer in the films was ALG, not c-ST; however, α -amylase enabled the film degradation.

The degradation behavior was also examined by ellipsometry (Fig. 4b). Upon just 5 min incubation of the multilayer films in

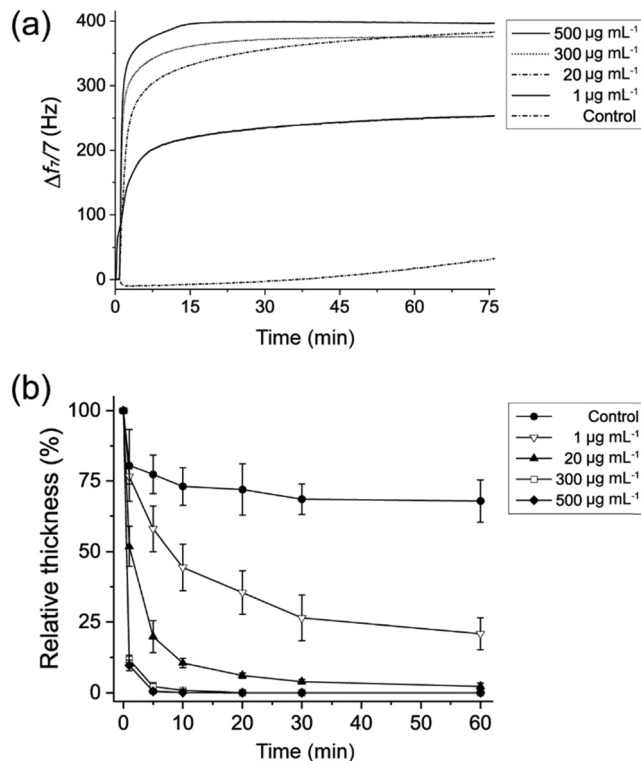


Fig. 4 Degradation profiles of [c-ST/ALG]₅ multilayer films after exposure to the α -amylase solutions at different concentrations: (a) QCM-D monitoring of $\Delta f_7/7$ vs. time and (b) thickness evolution measured by ellipsometry. Control: 0.1 M acetate buffer solution (pH 5.5).

the α -amylase solution at the highest concentration tested (500 $\mu\text{g mL}^{-1}$), 92% of the films were degraded. The degradation of the film was also enzyme-specific. Hyaluronidase and α -glucosidase, used as negative controls, were not capable of degrading the multilayer films. Thus, similarly to what was observed while using α -amylase-free 0.1 M acetate buffer solution (pH 5.5), these enzyme treatments caused no significant change in film thickness (Fig. S3, ESI[†]). The FT-IR and AFM characterizations further supported the successful α -amylase-driven, enzymatic degradation of the [c-ST/ALG]₅ multilayer films (Fig. S4 and S5, ESI[†]).

Controlled release of DNA

After confirming the enzymatic degradation of the [c-ST/ALG]₅ multilayer films, we investigated the enzyme-induced, biomolecule-release behavior from the films, for the potential application to stimuli-responsive drug delivery systems. Specifically, we incorporated DNA to the [c-ST/ALG]₄ multilayer films by performing an additional LbL process and formed the [c-ST/ALG]₄[c-ST/DNA]₃ multilayer films. The DNA release from the films was measured by fluorescent spectroscopy with bisBenzimide H 33258 (DNA detecting agent), after taking an aliquot at the predetermined incubation time. The result showed that most of the DNAs were rapidly released in 15 min upon the film exposure to the α -amylase solution (500 $\mu\text{g mL}^{-1}$), and the lower α -amylase concentration (20 $\mu\text{g mL}^{-1}$) slowed down the release rate (Fig. 5a). The results arguably confirmed that the DNA release was enzymatically controlled.

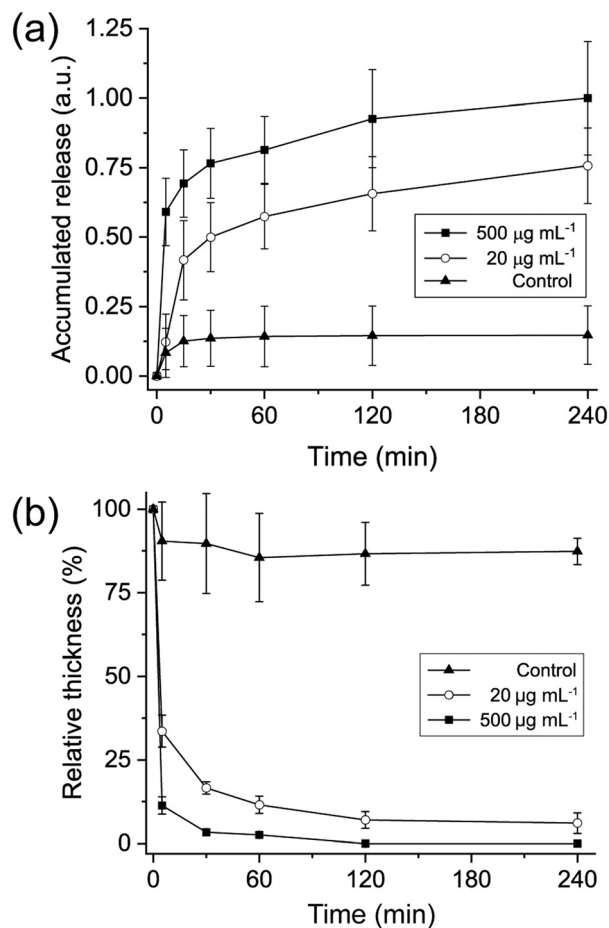


Fig. 5 Characterizations of DNA release from the [c-ST/ALG]₄[c-ST/DNA]₃ multilayer films: (a) accumulated amount of released DNA vs. degradation time and (b) relative thickness vs. degradation time.

The enzymatically triggered DNA release was additionally supported by the film-thickness changes. The thickness of the [c-ST/ALG]₄[c-ST/DNA]₃ films decreased to 11.4% in 5 min with 500 $\mu\text{g mL}^{-1}$ of α -amylase (Fig. 5b). The [c-ST/ALG]₄[c-ST/DNA]₃ films maintained about 87.4% of its original thickness (at the end of the assembly process) even after 240 min of exposure to the α -amylase-free 0.1 M acetate buffer solution (control experiment). Notably, the thickness reduction behavior of [c-ST/ALG]₄[c-ST/DNA]₃ showed a similar tendency to that of [c-ST/ALG]₅, indicating that the DNA molecule had a negligible effect on the film degradation. Taken all together, these results suggested that the α -amylase-triggered drug release system could be applied to various therapeutic compounds incorporated into the c-ST-based LbL films. In addition, this LbL-based drug delivery platform could be placed on various surfaces with complex geometries, like implantable devices, which find applications in a wide variety of biomedical scenarios.^{44,45} For example, the triggering enzyme, α -amylase, exists in the mouth and pancreas, and could be utilized for the target release *in vivo*.

Single-cell nanoencapsulation (SCNE)

Previous reports arguably indicate the intensive and wide use of the LbL process in the SCNE.^{6,7,46–48} The advantages of the LbL

methods in the SCNE include the potential in the formation of cyto-compatible nanoshells on individual living cells in a controlled mode, and the introduction of new functions that are not innate to the cells encapsulated. Various LbL pairs of biocompatible building blocks, such as chitosan or poly-L-lysine as cationic polymers and alginate or hyaluronic acid as anionic polymers, have so far been employed for the LbL-based SCNE.^{49–51} However, shell degradation still remains one of the missing pieces, because it is critically required that the conditions for shell degradation should be cyto-compatible, not doing any harm to living cells. Previous examples of degradable nanoshells in the SCNE could be found, such as the shells of metal-organic complex,^{52–55} but there have been no reports on LbL-based biodegradable shells. On-demand shell degradation is highly preferred, if not required, for increasing the applicability and use of the encapsulated cells.⁹

In the SCNE, the shell degradation should be triggered under cyto-compatible conditions, not to mention conditions for the shell formation. Based on the results gathered *via* QCM-D and ellipsometry, described in the previous sections, we thought that, if the c-ST/ALG multilayers were cyto-compatibly assembled on the cell surface, the c-ST-based LbL approach would be advantageously applied to the degradable SCNE: the films degraded rapidly under physiologically relevant conditions. We exploited the formation and enzymatic degradation of c-ST-based LbL nanoshells on individual *Saccharomyces cerevisiae* (baker's yeast) as a model system. *S. cerevisiae* was chosen since it had been widely used in the SCNE studies.⁵⁶

The c-ST-based LbL nanoshells were formed on the yeast, after priming the cells with Fe³⁺-TA complex, by following our previous protocol,⁵² in the PB solution (pH 5.8). For the easy visualization of the formed shells by confocal laser-scanning microscopy (CLSM), we used fluorescein-linked ALG (F-ALG) as an LbL component of the [c-ST/ALG]₄[c-ST/F-ALG]₃ multilayer shells. The CLSM images of the resulting encapsulated yeast, yeast@c-ST/ALG, clearly showed the ring-shaped, green fluorescence, confirming that c-ST and ALG (and F-ALG) were successfully deposited onto the cell surface, forming the c-ST/ALG nanoshells (Fig. 6a). After shell formation, the cyto-compatibility of the cell-forming process was investigated by the cell viability assay using FDA and PI. FDA has been used as a viability probe for measuring the intracellular esterase activity and cell-membrane integrity. PI intercalates between the bases in the intracellular DNA, which only happens with the cell membrane disintegration. The FDA-PI assay showed the viability of 97.6% after nanoshell formation (Fig. 6b), which was significantly higher than previously reported LbL-based SCNE studies with synthetic polymers. For instance, the LbL nanoshells, made of the multilayer films encompassing positively charged poly(allylamine hydrochloride) and negatively charged poly(styrenesulfonate), had 85% of viability even after 2-bilayer formation.^{57,58} In addition to the SCNE of *S. cerevisiae*, the cyto-compatibility of the c-ST/ALG films was examined by culturing NIH3T3 cells on the [c-ST]₅[ALG]₄ films (Fig. 7). The NIH3T3 cells adhered stably to the film and showed the high viability (99.57% at 1 day of culture), comparable to 99.39% of viability on the poly-D-lysine (PDL)-coated surface.

To investigate the biodegradability of the c-ST/ALG multilayer shells, yeast@c-ST/ALG was incubated for 10 min in the

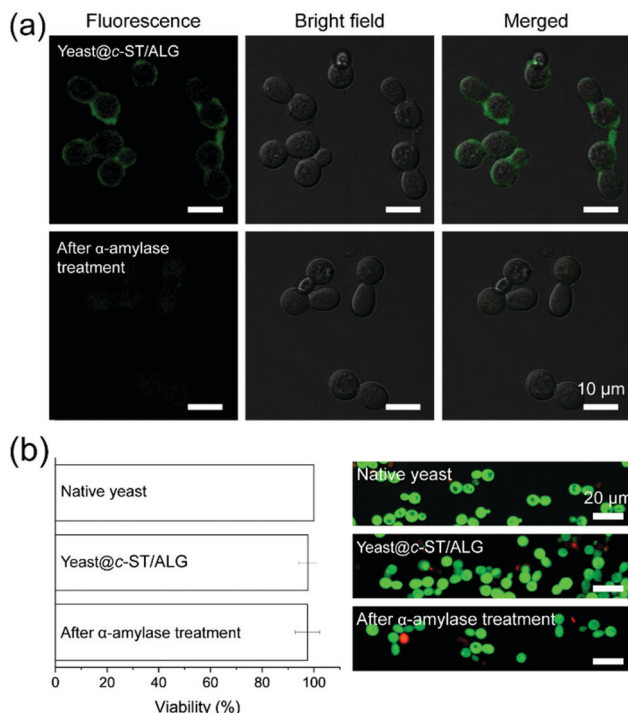


Fig. 6 Single-cell nanoencapsulation. (a) CLSM images of yeast cells (top) after shell formation and (bottom) after shell degradation. (b) Cell viabilities after shell formation and degradation. The encapsulated cells were treated with α -amylase ($500 \mu\text{g mL}^{-1}$) for 10 min. Green: live; red: dead.

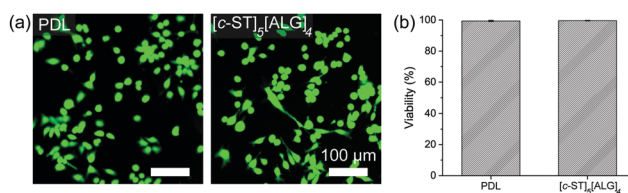


Fig. 7 Culture of NIH3T3 cells on the c-ST-based and PDL-coated surfaces. (a) CLSM images of the cells on PDL-coated and [c-ST]₅[ALG]₄ surfaces. Green: live; red: dead. Scale bars: 100 μ m. (b) Cell viability after 1 day of culture.

α -amylase solution ($500 \mu\text{g mL}^{-1}$ in the 0.1 M PB solution (pH 5.8)). After α -amylase treatment, no ring-shaped fluorescence was observed in the CLSM images, confirming the enzymatic degradation of the c-ST/ALG multilayer shells (Fig. 6a, right lower image). More importantly, the shell-degradation condition proved astonishingly cytocompatible: no noticeable decrease in the cell viability was observed after shell degradation (Fig. 6b). These results clearly confirmed that the c-ST-based LbL nanoshells were successfully assembled on and degraded from individual yeast in a highly cytocompatible manner, which is the first demonstration of degradable LbL nanoshells in the SCNE.

Conclusion

In conclusion, we have designed and fabricated ST-based LbL nanofilms, which showed an on-demand controlled degradability profile by the action of α -amylase, an ST-digestive enzyme. The

cytocompatible multilayer nanoshells, assembled *via* sequential adsorption of c-ST and ALG multilayers, were successfully formed on the surface of individual *Saccharomyces cerevisiae*, and the rapid shell degradation by α -amylase was achieved without any compromise in viability. The system demonstrated has several advantages in the SCNE field, in addition to the inherent ones standing out from the LbL approach *per se*, as follows: (1) the shell degradation is fast, requiring 10 min in the demonstrated case. Many previous works needed hours of incubation for shell degradation. The incubation time for shell degradation could be controlled more tightly in our system; (2) the conditions for shell degradation are strikingly cytocompatible. Because of the use of enzymes, the conditions ensure the complete cytocompatibility unless the degraded entities are cytotoxic. Other chemical methods could not compete with the enzymatic method; (3) cell viability upon the coating procedure is very high, indicating that one can easily and precisely tailor the thickness of the multilayer coating, as desired, by playing with the number of cycles of the LbL process without compromising the cell survival; (4) ST is cytocompatible and potentially yields the nutrients, maltose and glucose. The formation of degradable LbL films has used potentially toxic polymers, such as chitosan,^{59,60} which has antimicrobial activity and cannot be applied to the microbial SCNE. In addition, the degradation of ST into maltose and glucose would make the encapsulated cells survive in the nutrient-deprived conditions.

Although this work emphasizes the controlled enzyme-driven degradation of ST-based LbL nanofilms via α -amylase, there are many other ST-digestive enzymes derived from different sources in nature that could be employed. Therefore, we believe that the spatiotemporal control over assembly and disassembly would be made possible with the ST-based LbL architectures, offering a promising route in biomedical applications that require cytocompatible degradation *in vitro* and/or programmed dissolution *in vivo*.

Conflicts of interest

There are no conflicts to declare.

Acknowledgements

This work was supported by the Basic Science Research Program through the National Research Foundation of Korea (NRF) funded by the Ministry of Science, ICT & Future Planning (NRF-2018R1C1B5045778), Programa Operacional Regional do Centro – Centro 2020, in the component FEDER, and by national funds (OE) through FCT/MCTES, in the scope of the project “SUPRASORT” (PTDC/QUI-OUT/30658/2017, CENTRO-01-0145-FEDER-030658), as well as by the European Research Council grant agreement ERC-2014-ADG-669858 (ATLAS). J. Borges gratefully acknowledges FCT for the individual contract (CEECIND/03202/2017). This work was developed within the scope of the project CICECO-Aveiro Institute of Materials, UIDB/50011/2020 & UIDP/50011/2020, financed by national funds through the Foundation for Science and Technology/MCTES.

Notes and references

- 1 A. L. Becker, A. P. R. Johnston and F. Caruso, *Small*, 2010, **6**, 1836–1852.
- 2 K. Ariga, Y. M. Lvov, K. Kawakami, Q. Ji and J. P. Hill, *Adv. Drug Delivery Rev.*, 2011, **63**, 762–771.
- 3 K. C. Wood, J. Q. Boedicker, D. M. Lynn and P. T. Hammond, *Langmuir*, 2005, **21**, 1603–1609.
- 4 R. R. Costa and J. F. Mano, *Chem. Soc. Rev.*, 2014, **43**, 3453–3479.
- 5 R. F. Fakhrullin, A. I. Zamaleeva, R. T. Minullina, S. A. Konnova and V. N. Paunov, *Chem. Soc. Rev.*, 2012, **41**, 4189–4206.
- 6 I. Drachuk, M. K. Gupta and V. V. Tsukruk, *Adv. Funct. Mater.*, 2013, **23**, 4437–4453.
- 7 R. F. Fakhrullin and Y. M. Lvov, *ACS Nano*, 2012, **6**, 4557–4564.
- 8 J. H. Park, S. H. Yang, J. Lee, E. H. Ko, D. Hong and I. S. Choi, *Adv. Mater.*, 2014, **26**, 2001–2010.
- 9 J. H. Park, D. Hong, J. Lee and I. S. Choi, *Acc. Chem. Res.*, 2016, **49**, 792–800.
- 10 B. J. Kim, H. Cho, J. H. Park, J. F. Mano and I. S. Choi, *Adv. Mater.*, 2018, **30**, 1706063.
- 11 W. Youn, J. Y. Kim, J. Park, N. Kim, H. Choi, H. Cho and I. S. Choi, *Adv. Mater.*, 2020, DOI: 10.1002/adma.201907001.
- 12 W. Xiong, Z. Yang, H. Zhai, G. Wang, X. Xu, W. Ma and R. Tang, *Chem. Commun.*, 2013, **49**, 7525–7527.
- 13 S. H. Yang, K.-B. Lee, B. Kong, J.-H. Kim, H.-S. Kim and I. S. Choi, *Angew. Chem., Int. Ed.*, 2009, **48**, 9160–9163.
- 14 J. Lee, J. Choi, J. H. Park, M.-H. Kim, D. Hong, H. Cho, S. H. Yang and I. S. Choi, *Angew. Chem., Int. Ed.*, 2014, **53**, 8056–8059.
- 15 W. Youn, E. H. Ko, M.-H. Kim, M. Park, D. Hong, G. A. Seisenbaeva, V. G. Kessler and I. S. Choi, *Angew. Chem., Int. Ed.*, 2017, **56**, 10702–10706.
- 16 B. D. Ulery, L. S. Nair and C. T. Laurencin, *J. Polym. Sci., Part B: Polym. Phys.*, 2011, **49**, 832–864.
- 17 J. F. Mano, G. A. Silva, H. S. Azevedo, P. B. Malafaya, R. A. Sousa, S. S. Silva, L. F. Boesel, J. M. Oliveira, T. C. Santos, A. P. Marques, N. M. Neves and R. L. Reis, *J. R. Soc., Interface*, 2007, **4**, 999–1030.
- 18 T. Crouzier, T. Boudou and C. Picart, *Curr. Opin. Colloid Interface Sci.*, 2010, **15**, 417–426.
- 19 L. Richert, P. Lavalle, E. Payan, X. Z. Shu, G. D. Prestwich, J.-F. Stoltz, P. Schaaf, J.-C. Voegel and C. Picart, *Langmuir*, 2004, **20**, 448–458.
- 20 S. Boddohi and M. J. Kipper, *Adv. Mater.*, 2010, **22**, 2998–3016.
- 21 D. L. Elbert, C. B. Herbert and J. A. Hubbell, *Langmuir*, 1999, **15**, 5355–5362.
- 22 J. M. Silva, J. R. Garcia, R. L. Reis, A. J. Garcia and J. F. Mano, *Acta Biomater.*, 2017, **51**, 279–293.
- 23 T. Serizawa, M. Yamaguchi and M. Akashi, *Macromolecules*, 2002, **35**, 8656–8658.
- 24 R. R. Costa, C. A. Custódio, F. J. Arias, J. C. Rodríguez-Cabello and J. F. Mano, *Small*, 2011, **7**, 2640–2649.
- 25 F. Carosio, G. Fontaine, J. Alongi and S. Bourbigot, *ACS Appl. Mater. Interfaces*, 2015, **7**, 12158–12167.
- 26 Y. Zhang, C. Chi, X. Huang, Q. Zou, X. Li and L. Chen, *Carbohydr. Polym.*, 2017, **171**, 242–251.
- 27 A. K. Antosik, A. Piątek and K. Wilpiszewska, *Carbohydr. Polym.*, 2019, **222**, 115014.
- 28 H. F. Zobel, *Starch/Staerke*, 1988, **40**, 44–50.
- 29 R. F. Tester, J. Karkalas and X. Qi, *J. Cereal Sci.*, 2004, **39**, 151–165.
- 30 S. Hizukuri, Y. Takeda, M. Yasuda and A. Suzuki, *Carbohydr. Res.*, 1981, **94**, 205–213.
- 31 S. Hizukuri, *Carbohydr. Res.*, 1986, **147**, 342–347.
- 32 M. J. E. C. van der Maarel, B. van der Veen, J. C. M. Uitdehaag, H. Leemhuis and L. Dijkhuizen, *J. Biotechnol.*, 2002, **94**, 137–155.
- 33 A. Jiménez, M. J. Fabra, P. Talens and A. Chiralt, *Food Bioprocess Technol.*, 2012, **5**, 2058–2076.
- 34 J. Borges and J. F. Mano, *Chem. Rev.*, 2014, **114**, 8883–8942.
- 35 R. F. Fakhrullin, G. B. Sukhorukov and Y. M. Lvov, in *Handbook of Nanobiomedical Research: Fundamentals, Applications and Recent Developments*, ed. V. Torchilin, World Scientific, 2014, ch. 9, vol. 1, pp. 329–365.
- 36 I. Drachuk, O. Shchepelina, S. Harbaugh, N. Kelley-Loughnane, M. Stone and V. V. Tsukruk, *Small*, 2013, **9**, 3128–3137.
- 37 P.-X. Wang, X.-L. Wu, X. Dong-hua, X. Kun, T. Ying, D. Xi-bing and L. Wen-bo, *Carbohydr. Res.*, 2009, **344**, 851–855.
- 38 E. Hübsch, V. Ball, B. Senger, G. Decher, J.-C. Voegel and P. Schaaf, *Langmuir*, 2004, **20**, 1980–1985.
- 39 C. Porcel, P. Lavalle, V. Ball, G. Decher, B. Senger, J.-C. Voegel and P. Schaaf, *Langmuir*, 2006, **22**, 4376–4383.
- 40 M. J. Cardoso, S. G. Caridade, R. R. Costa and J. F. Mano, *Biomacromolecules*, 2016, **17**, 1347–1357.
- 41 K. Ren, J. Ji and J. Shen, *Biomaterials*, 2006, **27**, 1152–1159.
- 42 C. J. Ochs, G. K. Such and F. Caruso, *Langmuir*, 2011, **27**, 1275–1280.
- 43 O. Etienne, A. Schneider, C. Taddei, L. Richert, P. Schaaf, J.-C. Voegel, C. Egles and C. Picart, *Biomacromolecules*, 2005, **6**, 726–733.
- 44 M. P. Sousa, E. Arab-Tehrany, F. Cleymand and J. F. Mano, *Small*, 2019, **15**, 1901228.
- 45 X. Huang and C. S. Brazel, *J. Controlled Release*, 2001, **73**, 121–136.
- 46 M. B. Oliveira, J. Hatami and J. F. Mano, *Chem. – Asian J.*, 2016, **11**, 1753–1764.
- 47 R. T. Minullina, Y. N. Osin, D. G. Ishmuchametova and R. F. Fakhrullin, *Langmuir*, 2011, **27**, 7708–7713.
- 48 E. Rozhina, I. Ishmukhametov, S. Batasheva, F. Akhatova and R. Fakhrullin, *Beilstein J. Nanotechnol.*, 2019, **10**, 1818–1825.
- 49 M. Matsusaki, K. Kadowaki, Y. Nakahara and M. Akashi, *Angew. Chem., Int. Ed.*, 2007, **46**, 4689–4692.
- 50 I. Drachuk, R. Calabrese, S. Harbaugh, N. Kelley-Loughnane, D. L. Kaplan, M. Stone and V. V. Tsukruk, *ACS Nano*, 2015, **9**, 1219–1235.
- 51 D. Choi, H. Lee, H.-B. Kim, M. Yang, J. Heo, Y. Won, S. S. Jang, J. K. Park, Y. Son, T. I. Oh, E. Lee and J. Hong, *Chem. Mater.*, 2017, **29**, 2055–2065.
- 52 J. H. Park, K. Kim, J. Lee, J. Y. Choi, D. Hong, S. H. Yang, F. Caruso, Y. Lee and I. S. Choi, *Angew. Chem., Int. Ed.*, 2014, **53**, 12420–12425.

- 53 J. Lee, H. Cho, J. Choi, D. Hong, D. Kim, J. H. Park, S. H. Yang and I. S. Choi, *Nanoscale*, 2015, **7**, 18918–18922.
- 54 Z. Chen, H. Ji, C. Zhao, E. Ju, J. Ren and X. Qu, *Angew. Chem., Int. Ed.*, 2015, **54**, 4904–4908.
- 55 K. Liang, J. J. Richardson, J. Cui, F. Caruso, C. J. Doonan and P. Falcaro, *Adv. Mater.*, 2016, **28**, 7910–7914.
- 56 R. F. Fakhrullin, M.-L. Brandy, O. J. Cayre, O. D. Velev and V. N. Paunov, *Phys. Chem. Chem. Phys.*, 2010, **12**, 11912–11922.
- 57 J. Lee, S. H. Yang, S.-P. Hong, D. Hong, H. Lee, H.-Y. Lee, Y.-G. Kim and I. S. Choi, *Macromol. Rapid Commun.*, 2013, **34**, 1351–1356.
- 58 S. A. Konnova, I. R. Sharipova, T. A. Demina, Y. N. Osin, D. R. Yarullina, O. N. Ilinskaya, Y. M. Lvov and R. F. Fakhrullin, *Chem. Commun.*, 2013, **49**, 4208–4210.
- 59 E. I. Rabea, M. E.-T. Badawy, C. V. Stevens, G. Smagghe and W. Steurbaut, *Biomacromolecules*, 2003, **4**, 1457–1465.
- 60 K. W. Kim, R. L. Thomas, C. Lee and H. J. Park, *J. Food Prot.*, 2003, **66**, 1495–1498.